



PRESENTATION HANDOUT

NACDeC - VII

2023-2024

Team FlightForge

Aditya Singh^{1,†}, Kanak Agarwal^{1,†}

Parth Jain^{1,†}, Pranav Karkera^{1,†}

Vedant Vijayakrishnan^{1,†}

¹ Department of Aeronautical and Automobile Engineering, Manipal Institute of Technology, Manipal, Karnataka, India - 576104

† These authors contributed equally to this work.

1 The Problem Definition

The team's objective for this competition is to develop and propose a fully-fledged conceptual UAV for the planetary boundary layer (PBL) study of the lower stratum of the Martian atmosphere. The region of study for the proposed UAV would be the roughness layer corresponding to the initial 100 m above the Martian surface.

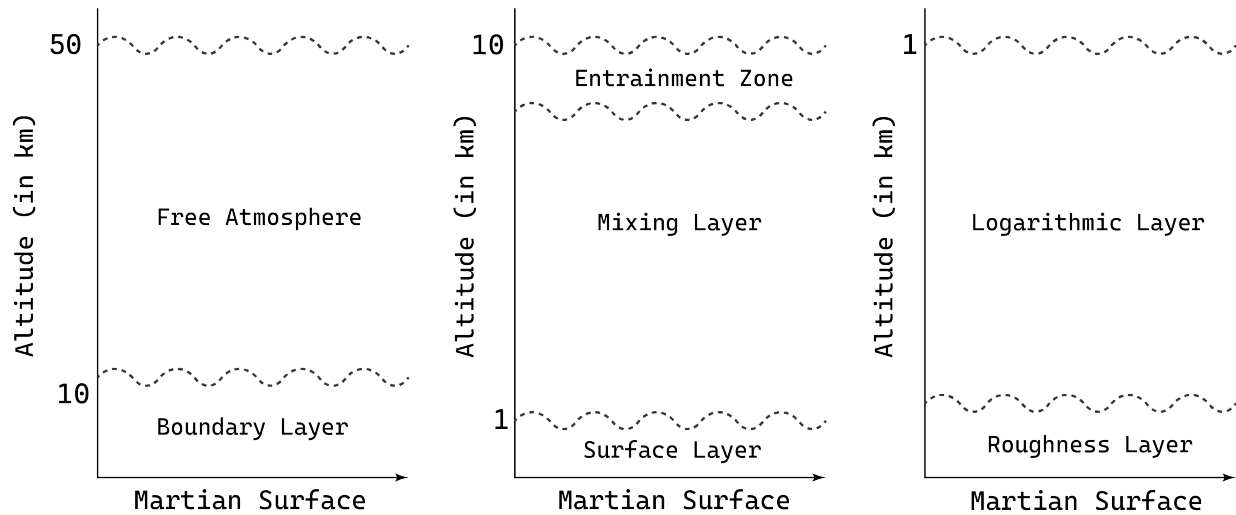


Figure 1: Martian Planetary Boundary Layer (PBL)

2 Preliminary Values Provided

The values provided initially as a part of the problem statement were taken as the starting point for the conceptual design process of the UAV.

| Parameter | Value | Parameter | Value |
|--|-----------------------------|---|----------------------|
| All up mass of the UAV | $\leq 70 \text{ kg}$ | Payload Mass | $\geq 5 \text{ kg}$ |
| Stowage Modularity | Aeroshell of Diameter 2.5 m | Waiting Period between two flights (after recharging) | 100 s |
| Battery Energy Density | 650 kJ/kg | Peak Irradiance on Mars (at 100 m) | 586.2 W/m^2 |
| Irradiance Attenuation Factor (at 100 m) | 0.70 | Length of a Martian Sol | 760 minutes |
| Reserve Battery Fraction after Each Flight | 25 % | Mass Fraction of the Battery Health Management System | 10 % |
| Mass Fraction of the Stowage System | 10 % | Mass Fraction of the Avionics System | 5 % |

Table 1: Preliminary Values

3 Timeline for the Competition

The requirements for each task were analysed. Post analysis, the work to be carried out was distributed across definite time frames using a Gantt chart in order to maximise productivity.

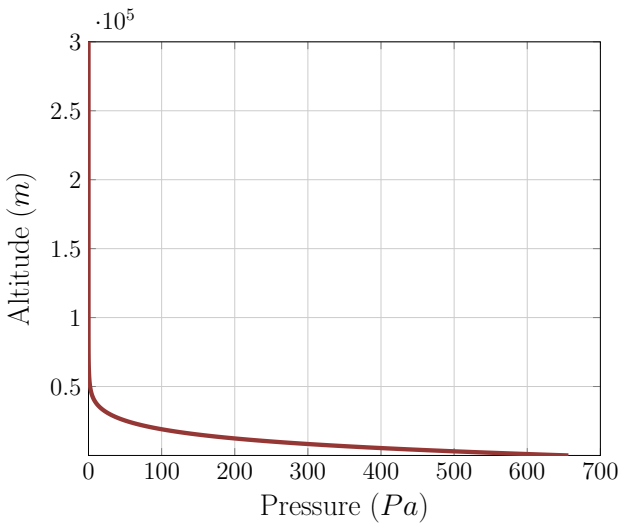
| | 2023 | | | 2024 | | | | | | | | | |
|-----------------------------|------|-----|-----|------|-----|-----|-----|-----|-----|------|-----|------|--|
| | Oct | Nov | Dec | Jan | Feb | Mar | Apr | May | Jun | July | Aug | Sept | |
| Initial Video Report | | | | | | | | | | | | | |
| Literature Survey | ■ | | | | | | | | | | | | |
| Irradiance Model | ■ | | | | | | | | | | | | |
| Reference Atmosphere | ■ | | | | | | | | | | | | |
| UAV Configurations | ■ | | | | | | | | | | | | |
| Design Challenges | ■ | | | | | | | | | | | | |
| Plan of Action | ■ | | | | | | | | | | | | |
| PPT and Video | ■ | | | | | | | | | | | | |
| Mid-Term Report | | | | | | | | | | | | | |
| Mission Profile | ■ | | | | | | | | | | | | |
| Sizing Methodology | ■ | | | | | | | | | | | | |
| Aerodynamic Analyses | ■ | | | | | | | | | | | | |
| Propulsive Analyses | ■ | | | | | | | | | | | | |
| Electrical Analysis | ■ | | | | | | | | | | | | |
| Vehicle Sizing | ■ | | | | | | | | | | | | |
| Mass Breakdown | ■ | | | | | | | | | | | | |
| Stowage Configuration | ■ | | | | | | | | | | | | |
| Report Writing | ■ | | | | | | | | | | | | |
| Final Report | | | | | | | | | | | | | |
| Final Configuration | ■ | | | | | | | | | | | | |
| 3D CAD Model | ■ | | | | | | | | | | | | |
| Sensitivity Analysis | ■ | | | | | | | | | | | | |
| Structural Design | ■ | | | | | | | | | | | | |
| CFD Analyses | ■ | | | | | | | | | | | | |
| Sortie Optimisation | ■ | | | | | | | | | | | | |
| EDL Analysis | ■ | | | | | | | | | | | | |
| Report Writing | ■ | | | | | | | | | | | | |
| Updated Report | | | | | | | | | | | | | |
| Presentation | ■ | | | | | | | | | | | | |

TODAY

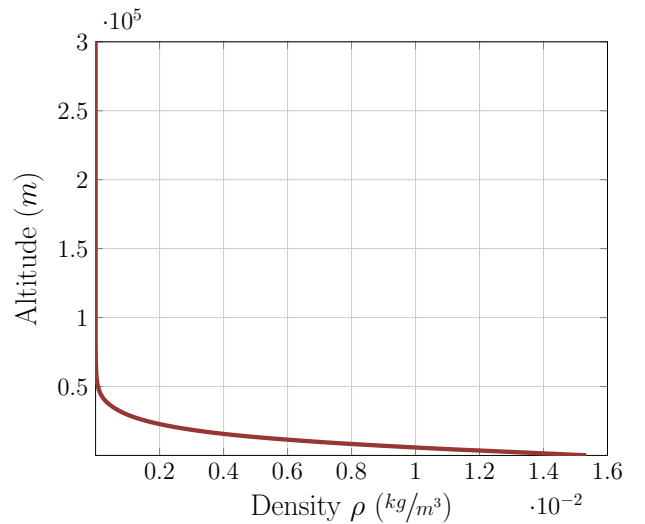
Figure 2: Timeline of the Competition

4 Martian Reference Atmosphere Model

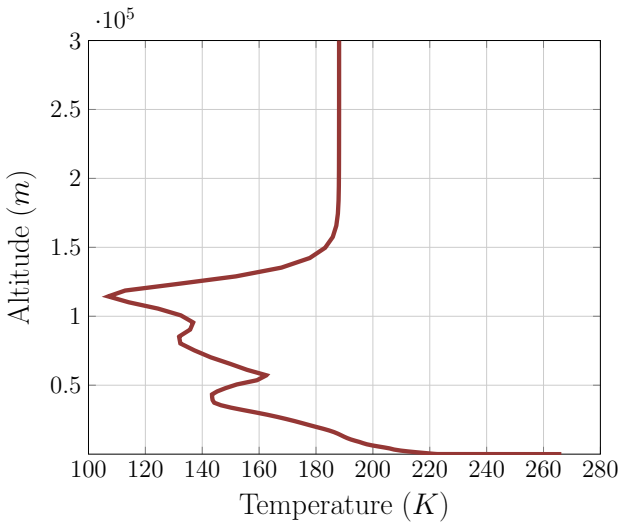
A Martian reference atmosphere was modelled using data from the Mars Climate Database, an open-source resource developed by several academic institutions in collaboration with the European Space Agency (ESA). The database, validated with data from Mars Years (MY) 24 to 35, aligns with the previous solar cycle. Based on observations and governing physical laws, these statistical models represent the current best understanding of the Martian atmosphere.



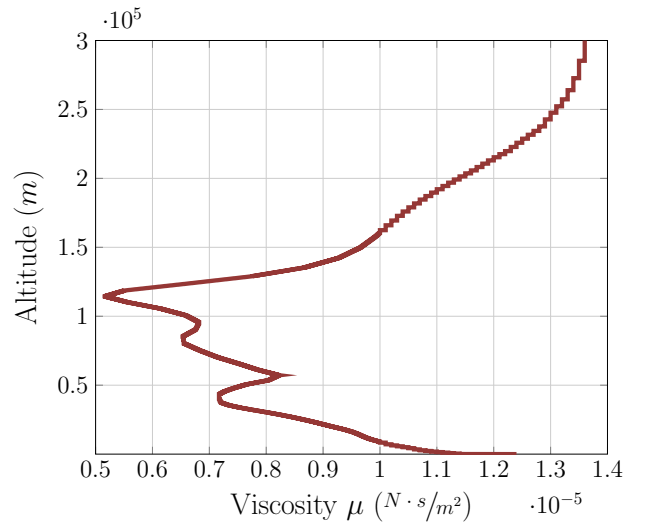
(a)



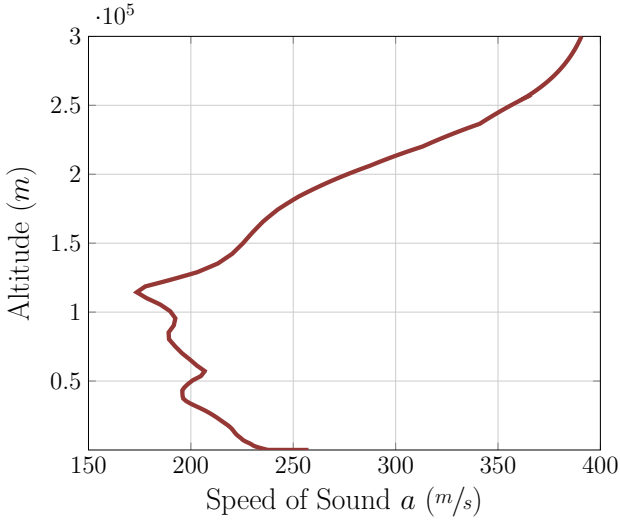
(b)



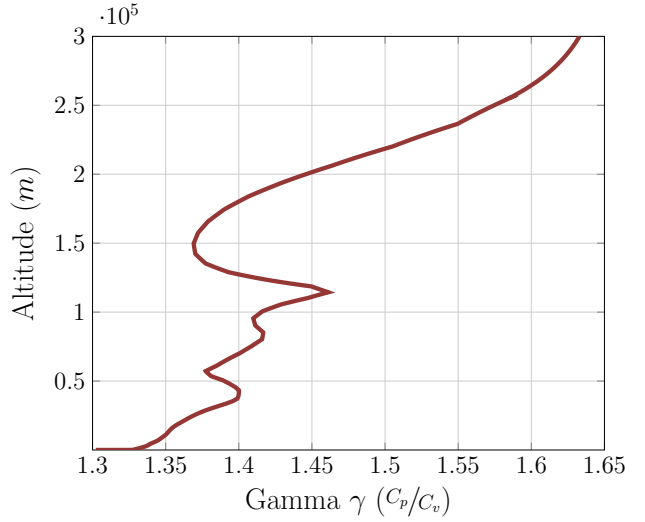
(c)



(d)



(e)



(f)

Figure 4: Martian Properties at constant Latitude & Longitude of 0° ,
Solar Longitude of 90° & Time = 12 hrs

5 Solar Irradiance Model

An irradiance model was created in MATLAB® after taking into consideration various parameters like the attenuation factor, latitude, Martian sol length and peak irradiance. The values used to model the solar irradiance are given below.

| Parameter | Value |
|--|---------------|
| Peak Irradiance on Mars (at 100 m) | 586.2 W/m^2 |
| Irradiance Attenuation Factor μ (at 100 m) | 0.70 |
| Length of a Martian Sol | 12.33 Hours |

Table 2: Preliminary Irradiance Values

The solar irradiance at the equator as a function of time, i.e., over the due course of the Martian day, is given in the figure below.

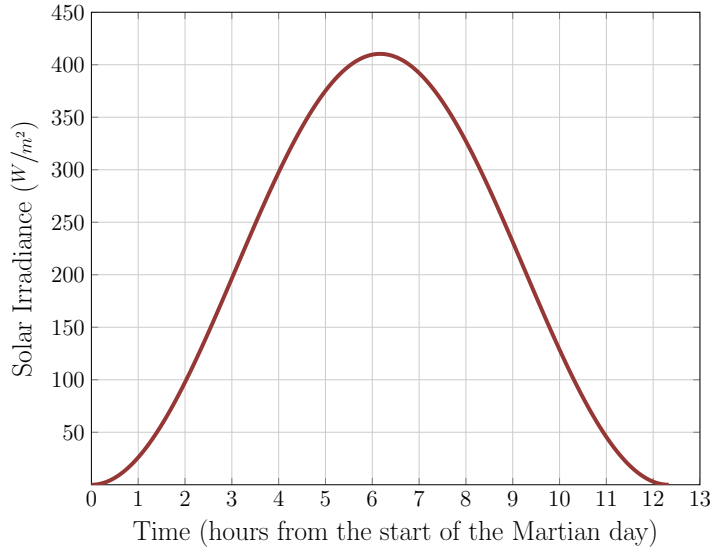


Figure 5: Variation of Solar Irradiance over the Martian Day

6 Preliminary Mission Profile

Initially, a preliminary mission profile was formulated. This helped to improve our understanding of the scope of the problem at hand.

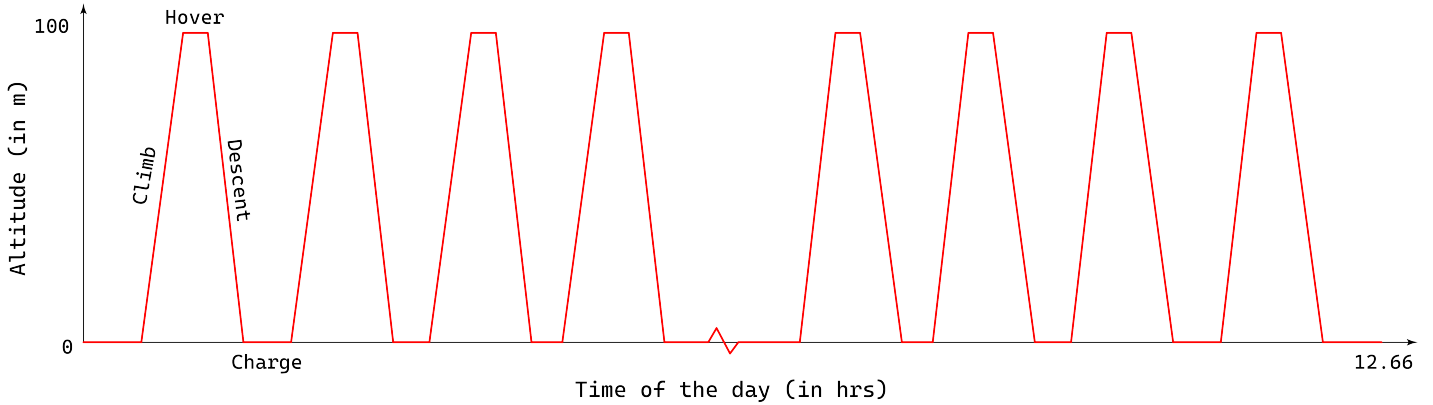


Figure 6: Preliminary Mission Profile

Some significant inferences drawn from the preliminary mission profile include:

- Charging time follows a parabolic trend, being shortest at noon and longest around sunrise and sunset.
- Flight time depends on ascent rate, descent rate, and hover time, with conventional (fixed-wing) UAVs achieving longer flight times compared to purely vertical (rotary) UAVs.

7 Coaxial UAV Configuration

The NASA Ingenuity UAV, a notable example of a coaxial rotor system, features a single motor with two rotors mounted on a concentric shaft, rotating in opposite directions to produce zero torque. This configuration generates significantly more thrust for a rotor radius similar to that of conventional helicopter setups. Coaxial UAVs are more compact, allowing better stowage, and can carry more payload with the same engine power. A coaxial system's low disk loading (Thrust/Rotor Area) enhances efficient hover and rotor thrust utilization, making it ideal for VTOL aircraft. Additionally, the system's increased stability in cross-wind conditions

is beneficial in Mars' dust storm-prone atmosphere, further justifying the choice of a coaxial single-rotor configuration.



Figure 7: The Ingenuity UAV

8 Design Methodology

The following flowchart details the sizing methodology incorporated throughout the design process.

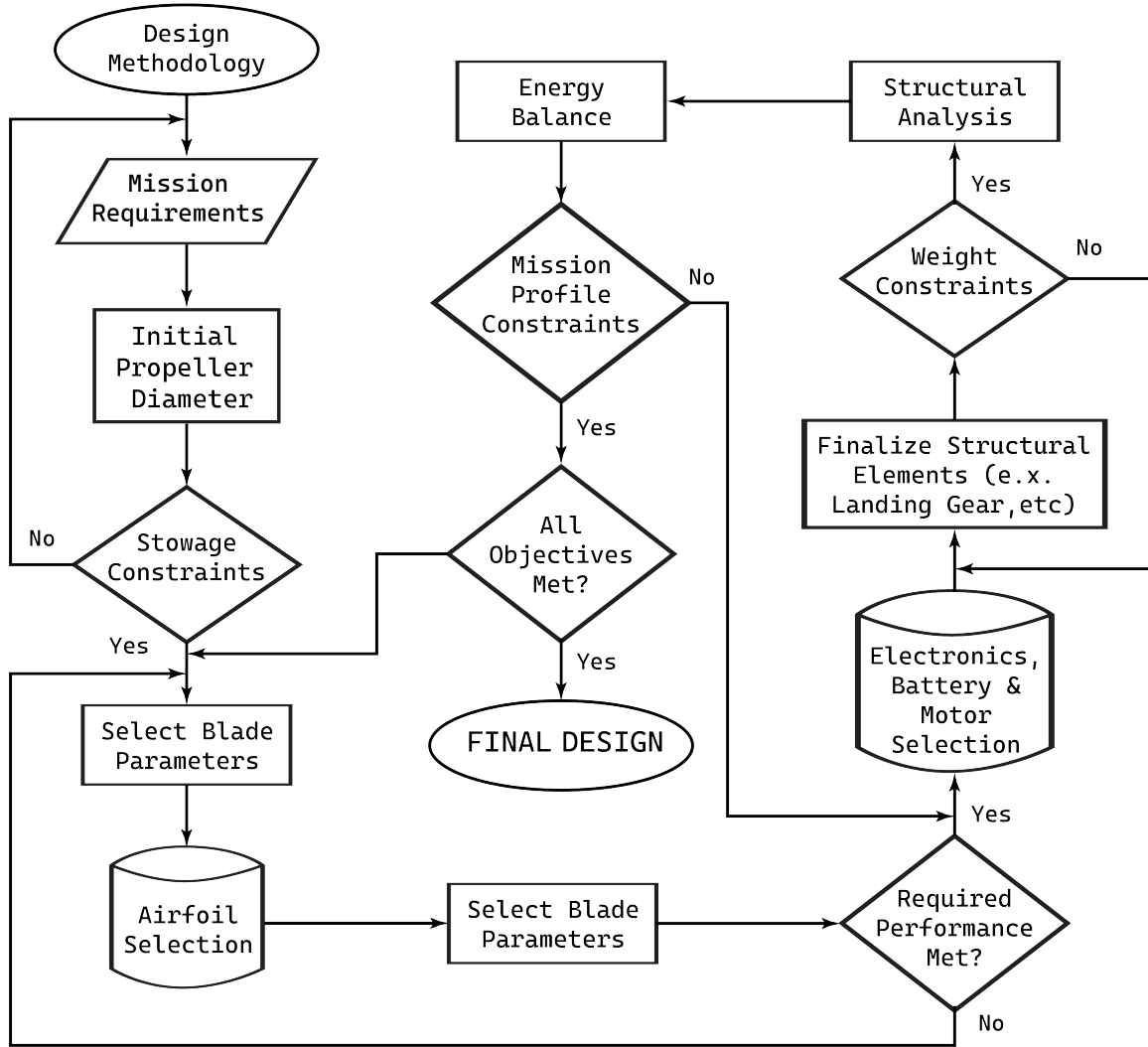


Figure 8: Design Methodology

9 Initial Sizing Constraints

The initial step in the sizing methodology was to estimate the propeller blade span, a critical parameter for subsequent analyses. A larger propeller span reduces disc loading (Thrust/Rotor Area), thereby lowering the

power required to hover, making it preferable. While propeller sizing involves many factors, stowage constraints primarily limit the propeller span in this case. The UAV must fit within an aeroshell with a 2.5 m diameter and 5 m height. Even if the propeller span exceeds the diameter, it can be folded using hinges at the blade roots. Given the unknown height of other structural elements, 2.5 m (50% of the aeroshell height) is allocated for stowing the propeller blades.

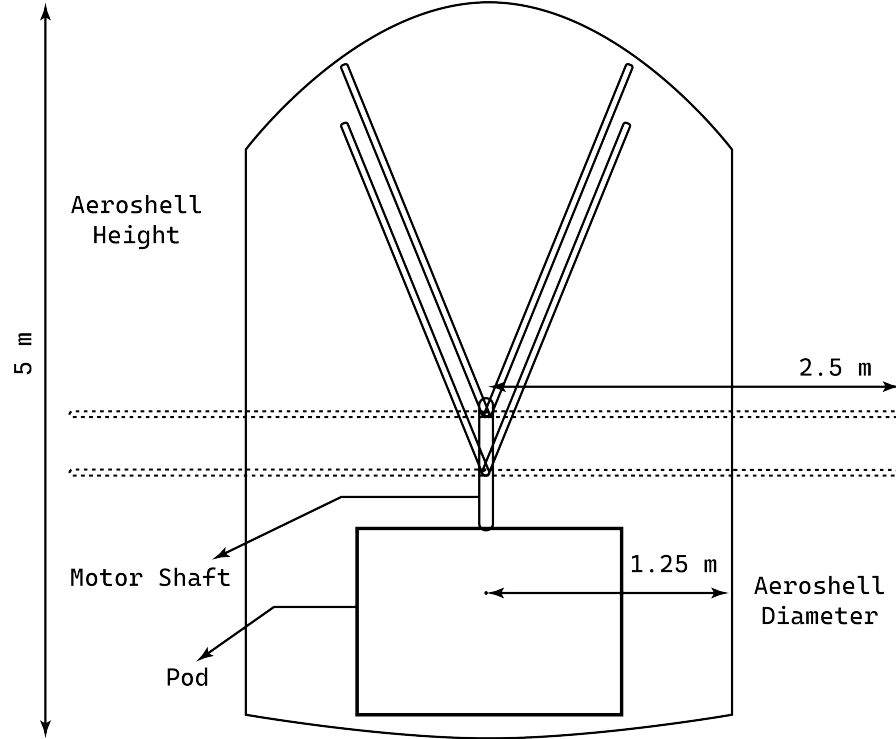


Figure 9: Proposed Stowage of the Propellers

10 Aerodynamic and Performance Analysis

10.1 Initial Constants

The table below depicts some of the initial constants and parameters assumed for this study.

| Parameter | Value |
|--|---|
| Mass, m | 70 kg |
| Acceleration due to Gravity, g_m | 9.81 m/s^2 |
| Thrust | 259.7 N |
| Average Speed of Sound, a_m | 343 m/s |
| Surface Density, ρ_m | $1.225 \times 10^{-3}\text{ kg/m}^3$ |
| Dynamic Viscosity, μ_m | $1.83 \times 10^{-5}\text{ Pas}$ |
| Kinematic Viscosity, ν_m | $1.83 \times 10^{-6}\text{ m}^2/\text{s}$ |
| Radius, R | 1.25 m |
| Propeller Actuator Disc Area, A | 19.635 m^2 |
| Tip Loss Factor, B | 0.98 |
| Empirical non-uniform flow correction factor, κ | 1.1 |

Table 3: Initial Constants and Parameters

10.2 Propeller Design

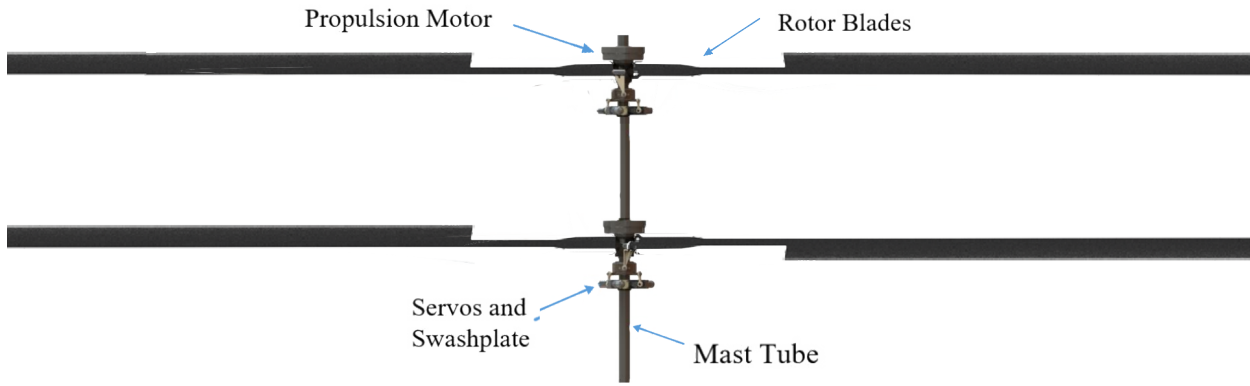


Figure 10: Propeller Configuration

| Parameter | Value |
|-----------------------------------|------------|
| Speed of sound, a_m | 240 m/s |
| Mach Constraint, M_{max} | 0.8 |
| Propeller Tip Velocity, V_{tip} | 192 m/s |
| Angular Velocity, Ω_{max} | 76.8 rad/s |
| Revolutions per second, RPS | 12.2231 /s |
| Revolutions per minute, RPM | 733.386 |
| Blade Aspect Ratio, AR | 25 |
| Blade Chord, c | 0.2 m |
| Number of blades (per rotor), b | 2 |
| Rotor Solidity (σ) | 0.0509 |

Table 4: Propeller Design Parameters

10.3 Airfoil Section

The airfoil section of the rotor is critical for blade performance, so its aerodynamic properties must be carefully examined. Maximizing the lift coefficient (C_l) while minimizing the drag coefficient (C_d) is key to achieving high aerodynamic efficiency. Traditional methods like XFOIL and XFLR5 fall short in predicting accurate aerodynamic coefficients, so Computational Fluid Dynamics (CFD) simulations were used instead. An optimal airfoil was selected after testing around 140 airfoils at various angles of attack. This airfoil, optimized for maximum performance under Martian conditions, is an interpolation between the NACA 6603 and Selig S1223 airfoils generated using XFLR5.



Figure 11: Airfoil

Its aerodynamic characteristics are given by,

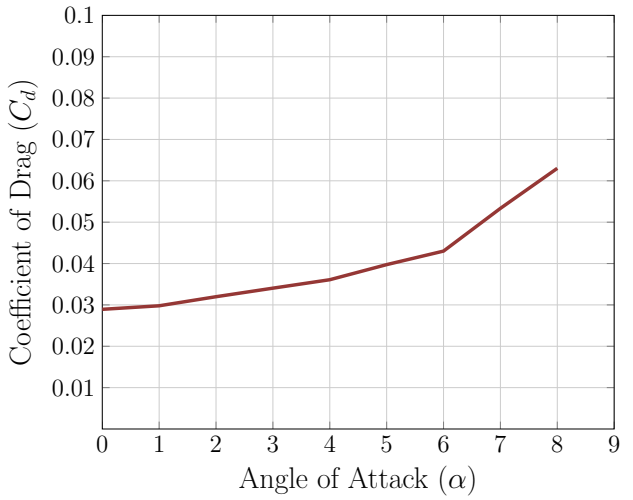
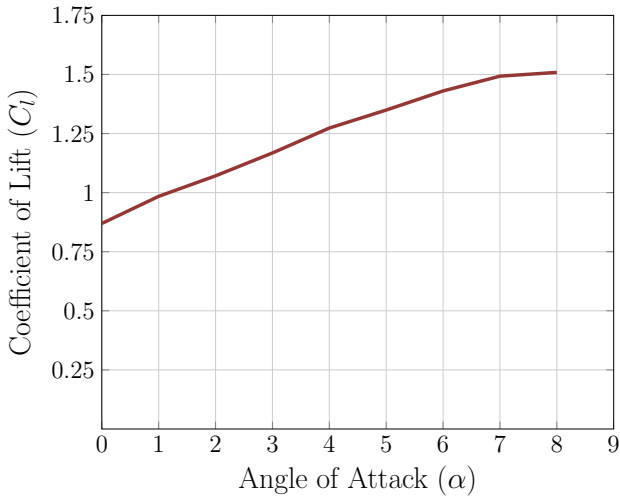


Figure 12: Aerodynamic Characteristics of the Selected Airfoil

10.4 Hover Performance

| Parameter | Value |
|---|------------------------|
| Propeller Separation Ratio, d_h | 0.08 |
| Propeller Separation, d | 0.4 m |
| Effective Area, A_e | 24.5124 m ² |
| Effective Radius, R_e | 2.7933 m |
| Induced velocity, v_{i_h} | 18.7924 m/s |
| Induced Power (Hover), P_i | 4880.4 W |
| Induced Power (single rotor with r = 2.5 m) | 5453 W |

Table 5: Hover Parameters

The following plots illustrate how varying the number of blades and other parameters affect the total hover power.

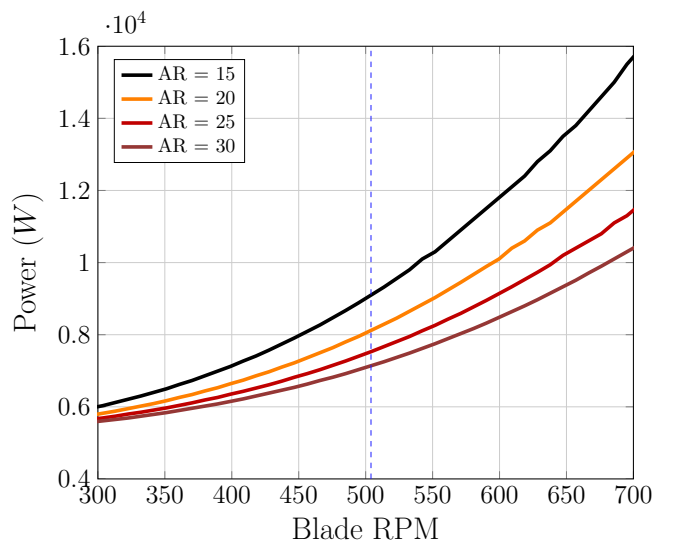
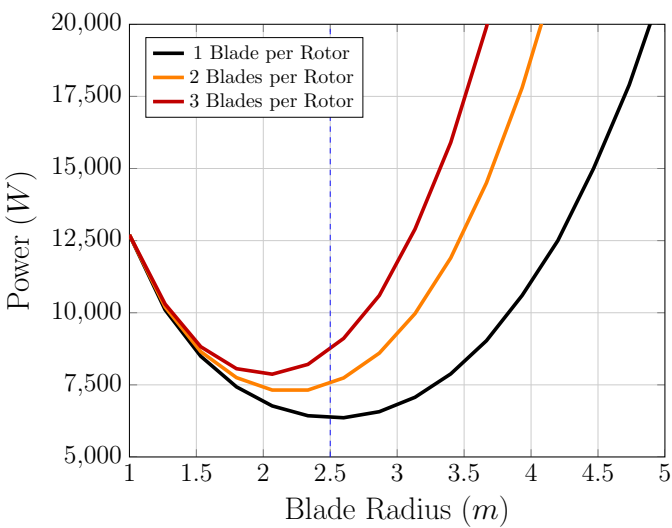


Figure 13: Variation of Power with Blade Radius & RPM

10.5 Performance and Aerodynamic parameters

| Parameter | Expression | Value |
|--------------------------------------|--|-------------------------|
| Thrust Coefficient, C_T | $T/(\rho A_e (R_e \Omega_{hover})^2)$ | 0.0325 |
| Blade Solidity, σ | $bc/\pi R$ | 0.0509 |
| Power Coefficient, C_P | $P_t/(\rho A_e (R_e \Omega_{hover})^3)$ | 0.0066 |
| Induced Power Coefficient, C_{P_i} | $P_i/(\rho A_e B (R_e \Omega_{hover})^3)$ | 0.0042 |
| Power-Solidity Ratio, CPS | C_P/σ | 0.1305 |
| Power Loading, PL | C_T/C_P | 4.89 |
| Disk Loading, DL | $T/(2 \times A)$ | 6.6132 N/m ² |
| Inflow Ratio, λ | $\sqrt{C_T/2}$ or $v_{i_h}/(\Omega_{hover} R)$ | ≈ 0.11 |
| Figure of Merit, FOM | $C_T^{3/2}/(\sqrt{2} C_P)$ | ≈ 0.6234 |

Table 6: Hover performance and Aerodynamic parameters

10.6 Validation

To validate our initial approximations, we compared them with values obtained from an online technical calculator that provides helicopter performance parameters.

| Parameter | Calculated (Momentum Theory) | Reference Calculator | Error (%) |
|-----------------------------|------------------------------|----------------------|-----------|
| Induced velocity, v_{i_h} | 18.7924 m/s | 18.757 m/s | 0.2 % |
| Total Power (Hover), P_i | 7823 W | 8426.4 W | 7.8 % |

Table 7: Hover Parameters Validation

The difference in total power values can be attributed to the inclusion of tail rotor power in the calculations, which typically accounts for about 10% of the total hover power in most conventional helicopters.

10.7 Vertical Flight

Vertical flight consists of hover ($V=0$), climb ($V>0$), and descent ($V<0$), where V represents the rate of climb. The variation in the rate of climb/descent (V) with varying angles of attack is shown below,

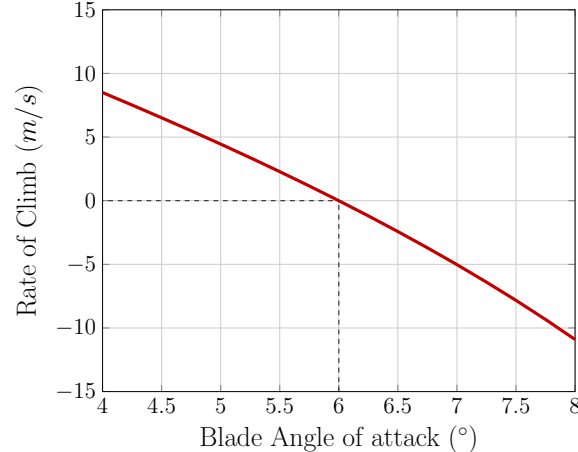


Figure 14: Rate of Climb v/s Blade Angle of Attack

The following graph illustrates how the different components of the total power vary with changes in the rate of climb.

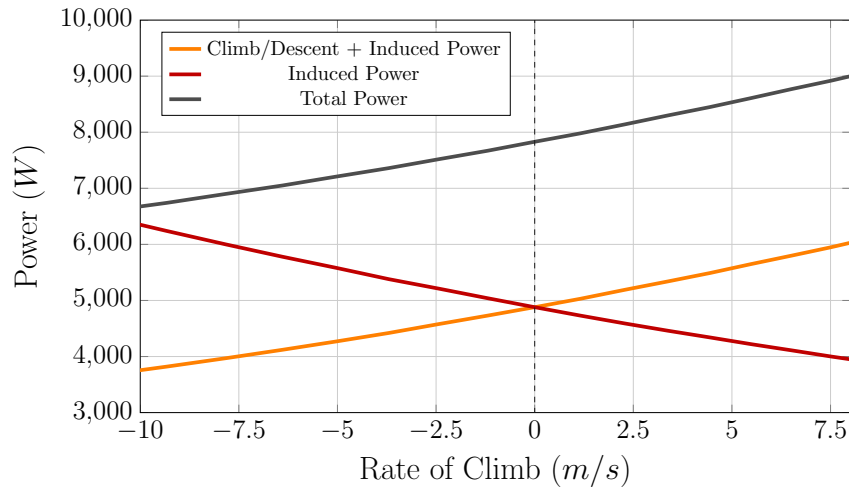


Figure 15: Power consumption v/s Rate of Climb

The rate of climb as a function of only the excess power produced by the motor is compared with the rate of climb observed by varying the angle of attack from our formulation,

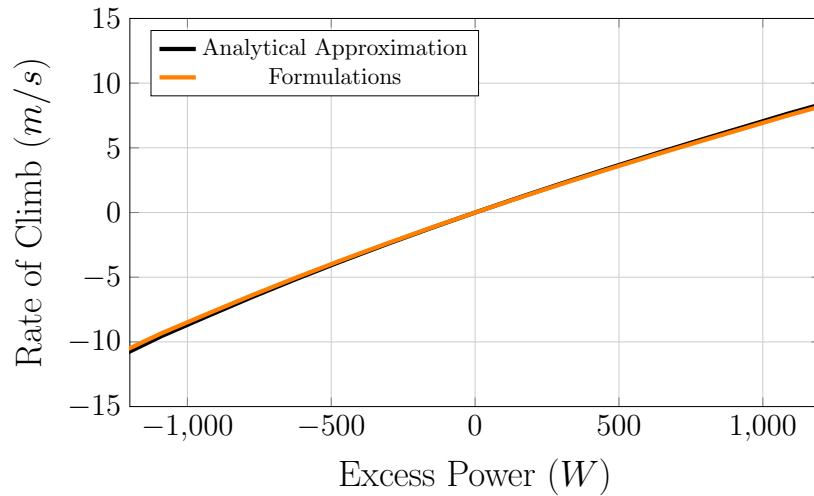


Figure 16: Rate of Climb v/s Excess Power

The variation of the climbing power to hovering power ratio for different rates of climbs is shown below,

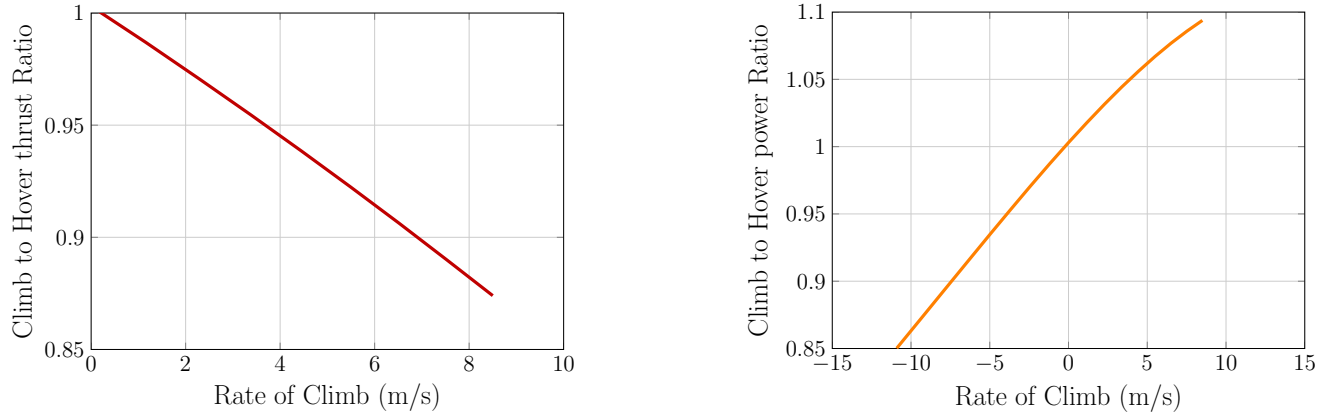


Figure 17: Thrust & Power Ratio v/s Rate of Climb

10.8 Forward Flight

The plot of the total power consumed by the helicopter at different forward speeds is shown below.

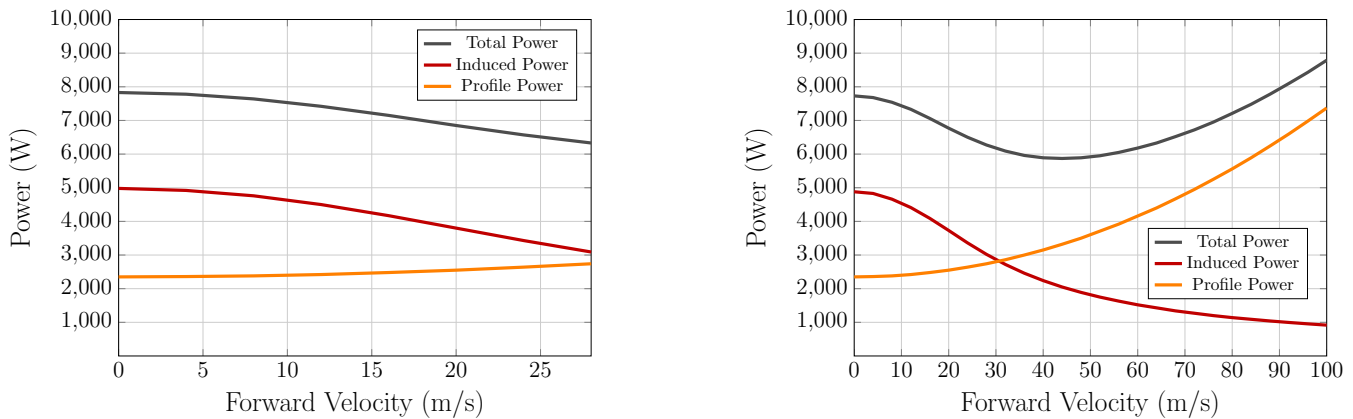


Figure 18: Variation of Total Power with Forward Velocity

The variation of the range and the endurance of the UAV with forward velocity is illustrated below,

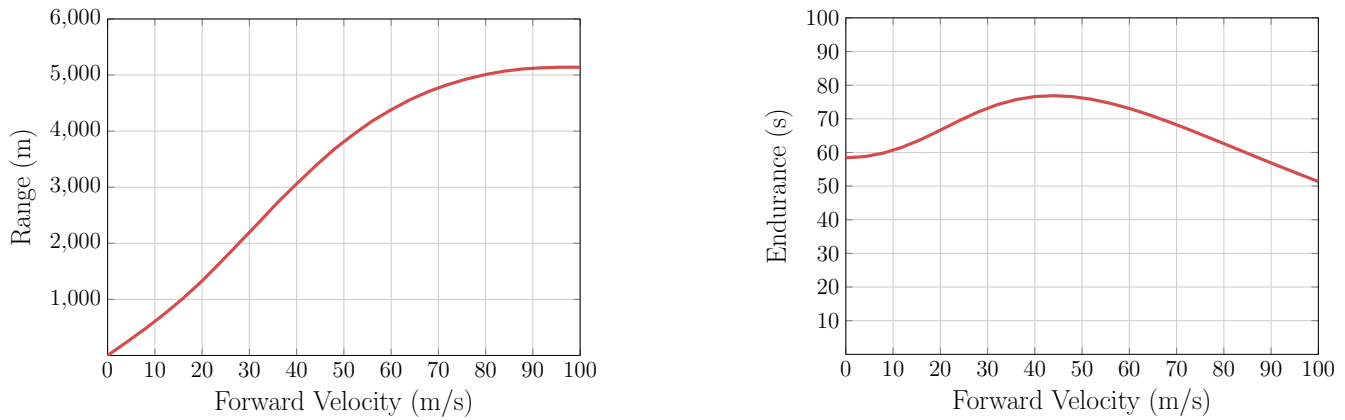
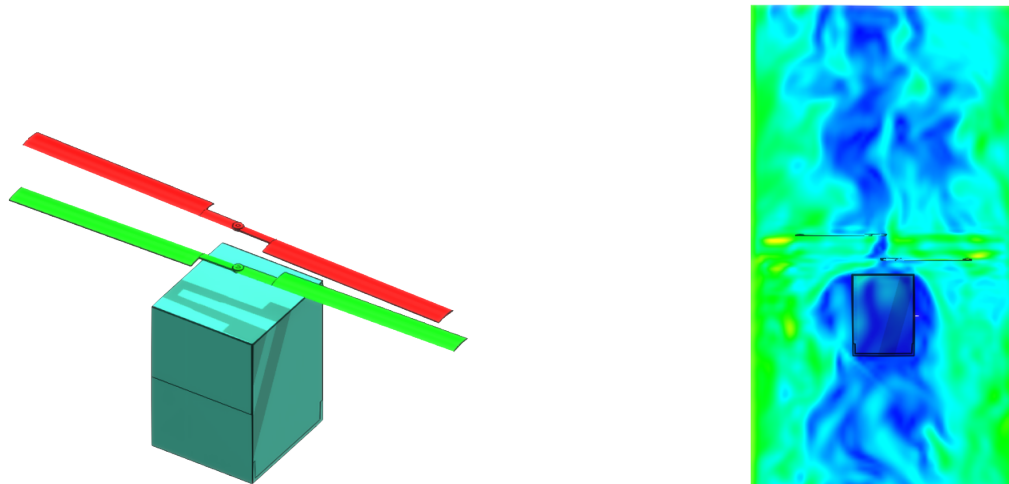


Figure 19: Variation of Range and Endurance with Forward Velocity

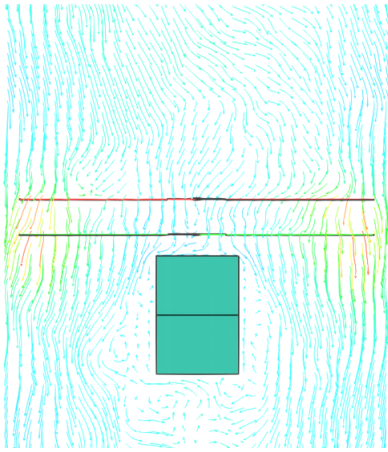
10.9 Propeller Wake Analysis

A comprehensive turbo-machinery unsteady CFD analysis was carried out using the commercially available Simulia XFlow software to study the wake produced by the propeller blades.

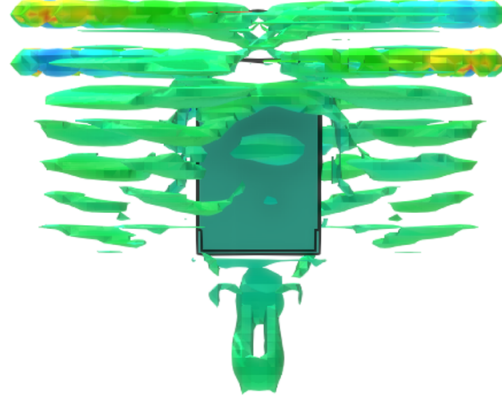


(a) Simulation Model

(b) Induced Velocity



(c) Total Pressure

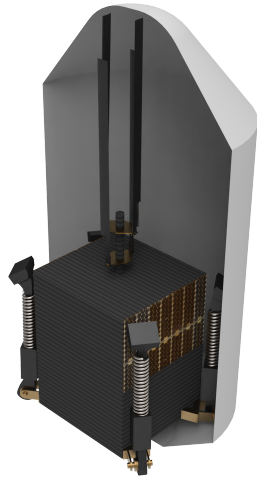


(d) Vortex Core Region

Figure 21: CFD Results

11 Stowage Analysis

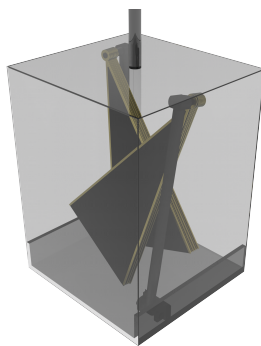
In order to maximise the usage of the provided aeroshell, a folding mechanism is used for the propellers and the solar panel. By folding the propellers upwards, we are able to maximise the usage of the given 5 m aeroshell height.



(a) UAV Stowage



(b) Dimensions of payload fairing



(c) Folded Solar Array



(d) Shutter Mechanism

Figure 22: Stowage Analysis

12 Final Configuration

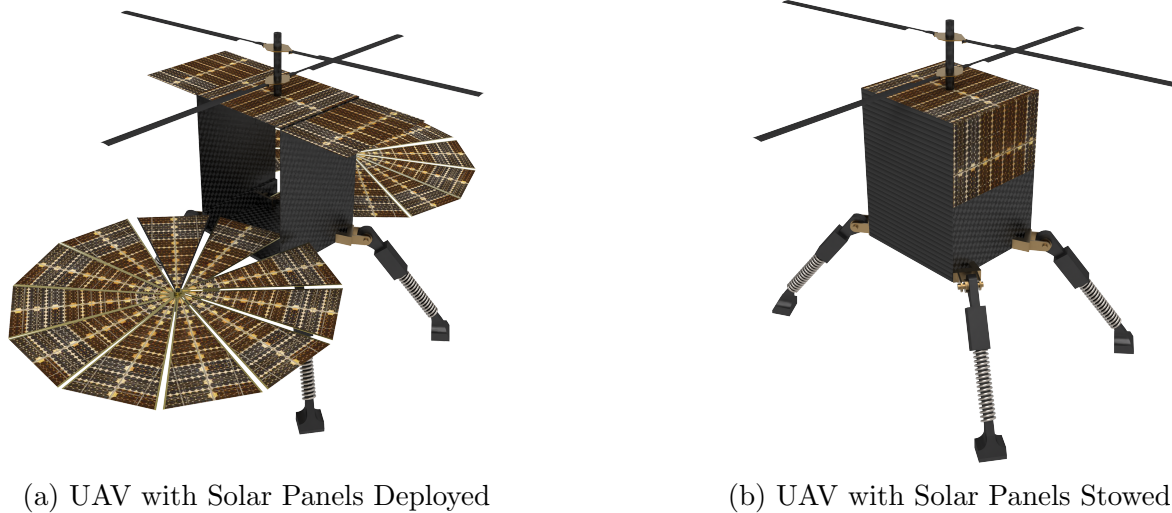


Figure 23: Final UAV Configuration

13 Structural Analysis

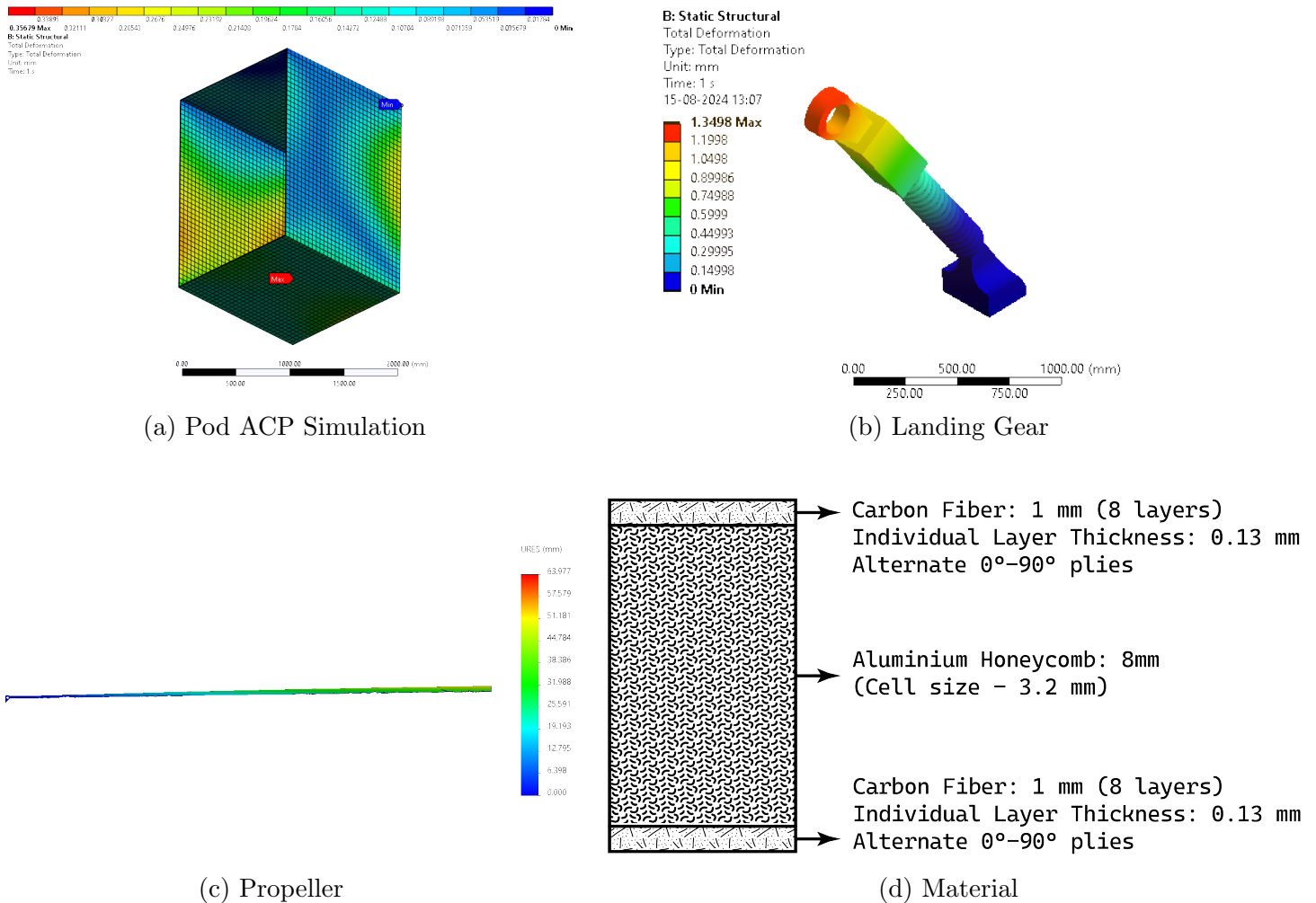


Figure 24: Structural Analysis

14 Electronics

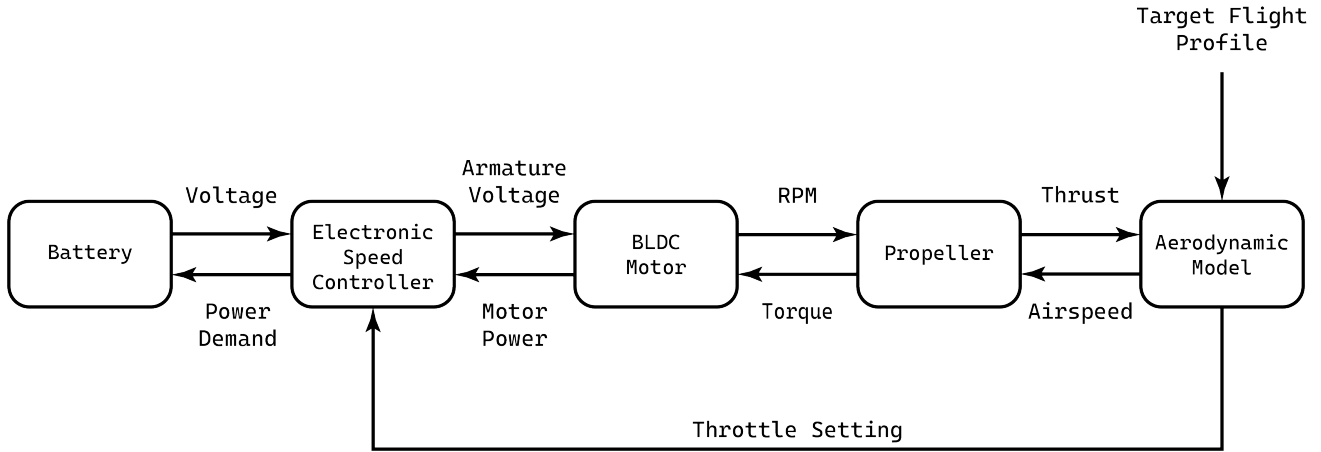


Figure 25: UAV Power Model Block Diagram

14.1 Solar Panel

Second-generation solar cells were selected for the mission due to their low mass density and minimal material requirements, thanks to their thin-film structure. Common semiconductor materials for thin films include amorphous silicon (a-Si), cadmium telluride (CdTe), CIGS (copper indium gallium selenide), and organic polymers, all of which offer advantages like low weight and cost efficiency. However, only CIGS cells provide the required conversion efficiency (15-20%), while a-Si and CdTe cells have much lower efficiency ($\leq 10\%$), making CIGS the optimal choice for the mission.

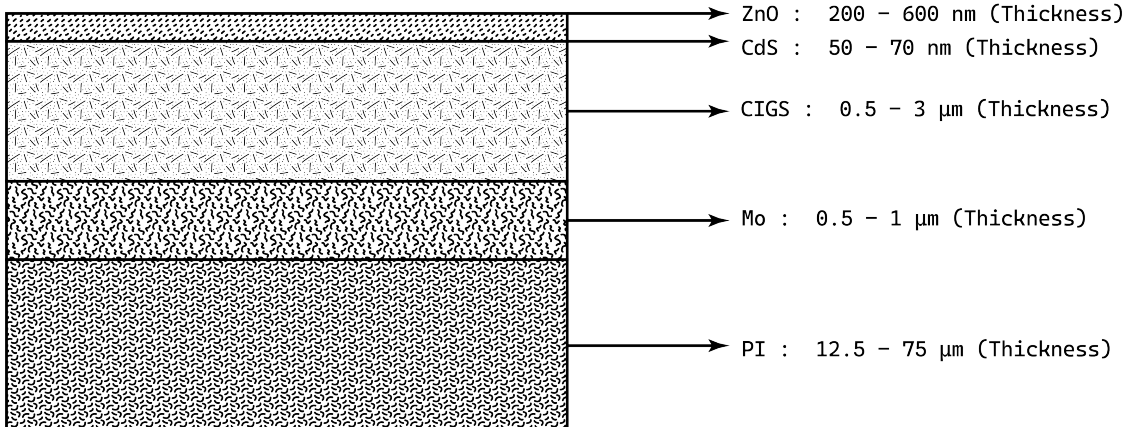


Figure 26: Schematic of the Solar Cell Structure

| Layer | Material | Thickness |
|------------------------------|--------------------------------|---------------------|
| Substrate Layer | Polyamide | 75 μm |
| Back Contact Layer | Molybdenum | 2 μm |
| Semiconductor Absorber Layer | Copper Indium Gallium Selenide | 3 μm |
| Buffer Layer | Cadmium Sulfide | 70 nm |
| Front Contact Layer | Zinc Oxide | 600 nm |
| Total Thickness | | 80.67 μm |

Table 8: Description of the Solar Cell Layer

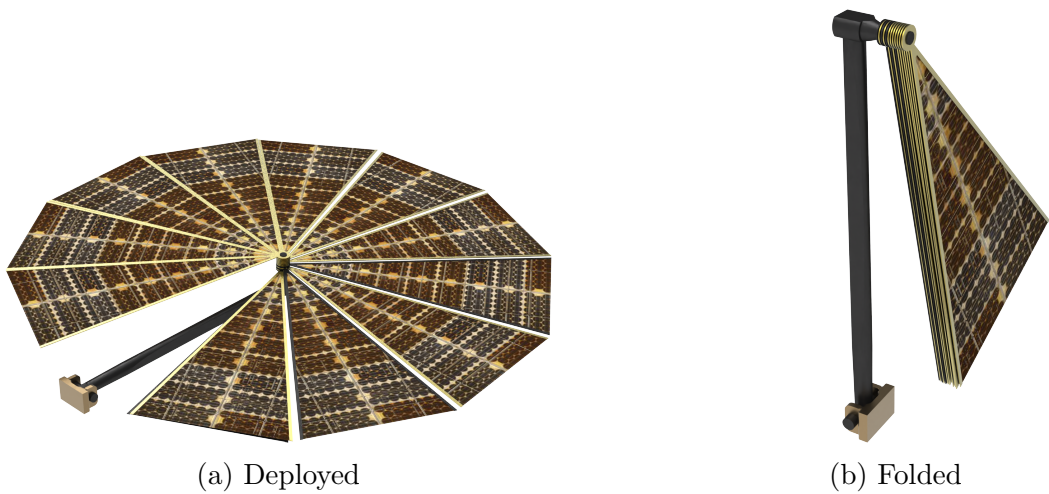


Figure 27: Solar Panel Mechanism

14.2 Battery

| Parameter | Value |
|----------------------------|--------------------------------|
| Energy Density | 650 kJ/kg (180 Wh/kg) |
| Number of Battery Packages | 2 |
| Battery Mass | $2 \times 1.5 kg$ |
| Total Energy Capacity | $2 \times 270 Wh$ |
| Max. Depth of Discharge | 75% |
| Packing Configuration | 24S |
| Working Voltage | 100 V |
| Battery Ah Rating | $2 \times 2.7 Ah$ |
| Charge C Rating | 1 |
| Discharge C Rating | 20 |
| Cycle Life | ≥ 300 |
| Dimensions | 108 mm x 108 mm x 190 mm |

Table 9: Battery Parameters

14.3 Motor

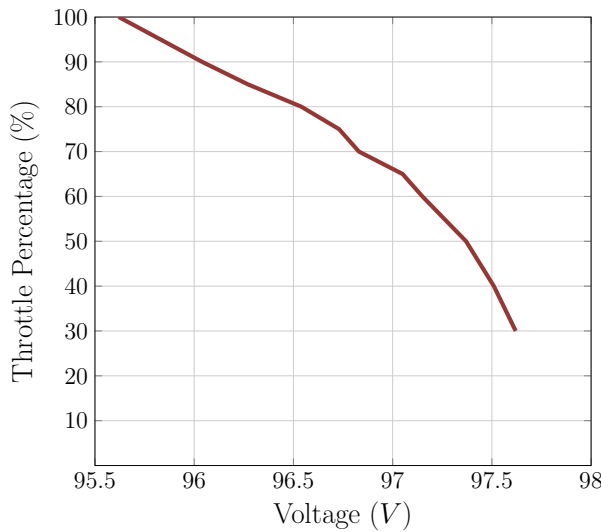


Figure 28: Motor Specifications

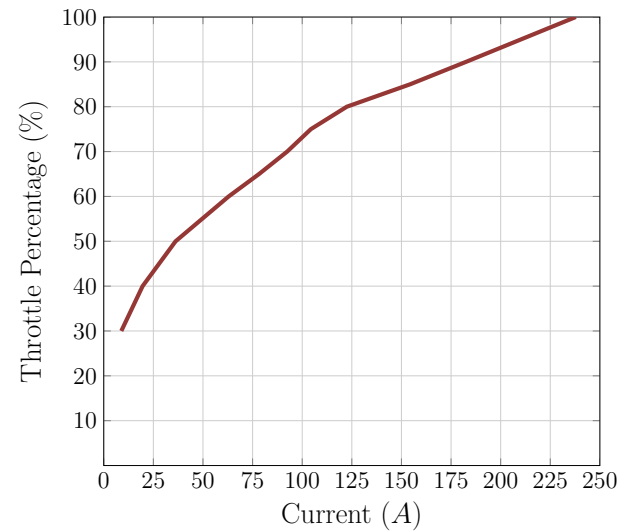
| Parameter | Value |
|----------------------------|---------------------------|
| KV Rating | 43 |
| Mass | $2 \times 2.5 \text{ kg}$ |
| Configuration | 36N30P |
| Max. Current | 238 A |
| Nominal Voltage | 24S |
| Internal Resistance | $20.3 \text{ m}\Omega$ |
| Max. Power | 23 kW |
| Max. Torque | 47.7 N - m |
| Max. Operating Temperature | 125 °C |

Table 10: Motor Specifications

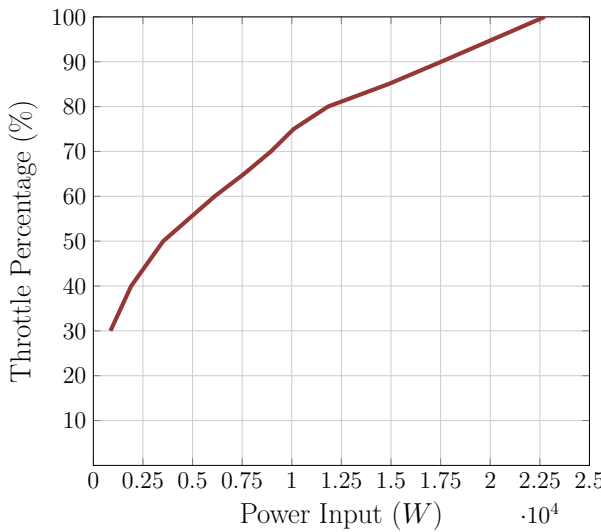
The following graphs showcase the trend of various operational motor parameters.



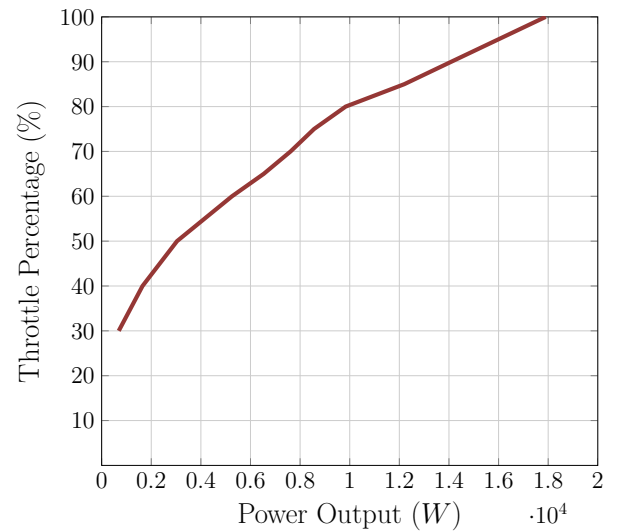
(a)



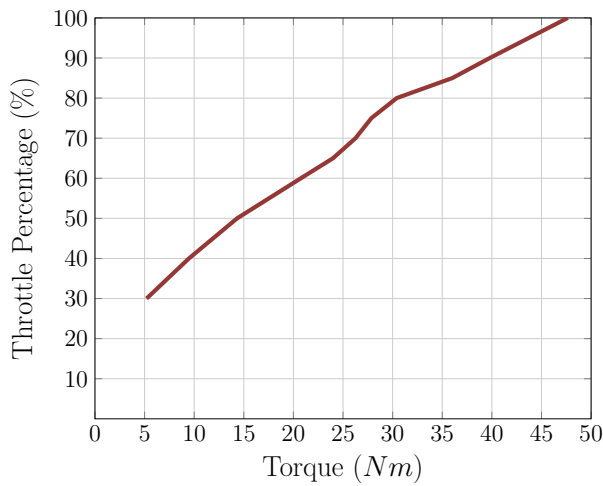
(b)



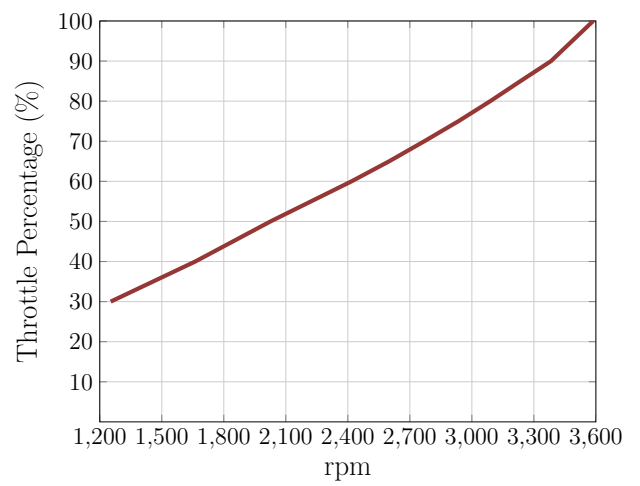
(c)



(d)



(e)



(f)

Figure 30: Motor Performance

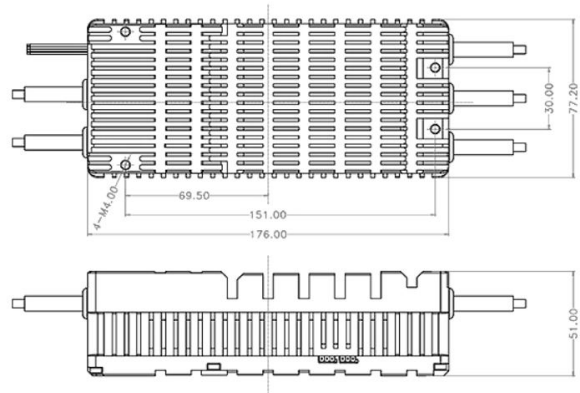
| Throttle (%) | Voltage (V) | Current (A) | Input Power (W) | Output Power (W) | Torque (N-m) | RPM | Efficiency (%) |
|--------------|-------------|-------------|-----------------|------------------|--------------|------|----------------|
| 30 | 97.62 | 8.85 | 863.9 | 689.4 | 5.2 | 1253 | 79.8 |
| 40 | 97.51 | 19.58 | 1909.2 | 1647.7 | 9.468 | 1662 | 86.3 |
| 50 | 97.37 | 36.2 | 3524.8 | 3038.4 | 14.322 | 2026 | 86.2 |
| 60 | 97.15 | 62.96 | 6116.6 | 5254.1 | 20.75 | 2418 | 85.9 |
| 65 | 97.05 | 78.27 | 7596.1 | 6532.6 | 23.99 | 2600 | 85.1 |
| 70 | 96.83 | 92.43 | 8950 | 7616.4 | 26.26 | 2770 | 85.1 |
| 75 | 96.73 | 104.38 | 10096.7 | 8562 | 27.86 | 2935 | 84.8 |
| 80 | 96.54 | 122.47 | 11823.3 | 9836.9 | 30.41 | 3089 | 83.2 |
| 85 | 96.27 | 154.38 | 14862.2 | 12201.8 | 36.02 | 3235 | 82.1 |
| 90 | 96.04 | 182.54 | 17531.4 | 14095 | 39.79 | 3383 | 80.4 |
| 100 | 95.62 | 237.86 | 22744.2 | 17899.7 | 47.65 | 3587 | 78.7 |

Table 11: Theoretical Motor Data

14.4 Electronic Speed Controller (ESC)



(a) ESC



(b) ESC Dimensions

Figure 31: Electronic Speed Controller (ESC)

The specifications of the ESC are shown below.

| Parameter | Value |
|------------------------------|--------------------------|
| Current Limit | 300 A |
| Supported Lithium Cell Count | 12-24S |
| Throttle Loss Protection | Supported |
| Temperature Protection | Supported |
| Compatible Signal Frequency | 50-500 Hz |
| Operating Temperature | -20°C to 65°C |
| Dimensions | 176 mm × 77.2 mm × 52 mm |
| Mass (excl. wires) | 0.975 kg |

Table 12: ESC Specifications

14.5 Payload Sensors

The mission aims to study the deep Martian boundary layer using high-resolution vertical profiling. The payload will include several sensors that will carry out high-resolution vertical profiling.

Temperature Sensor: The sensor is essential for capturing temperature profiles, which helps in understanding thermal processes, atmospheric stability, and vertical transport in the Martian boundary layer. It uses a small bead thermistor for precise measurements, weighs 0.15 kg, and requires about 0.5 W of power.



Figure 32: Spherical Bead Thermistors

Pressure Sensor: The sensor is vital for studying global atmospheric dynamics, topography-driven pressure effects, CO₂, and dust cycles. It features a micro-machined capacitive pressure sensor and transducer electronics for precise vertical pressure measurements. It weighs 0.04 kg and requires about 0.015 W of power.

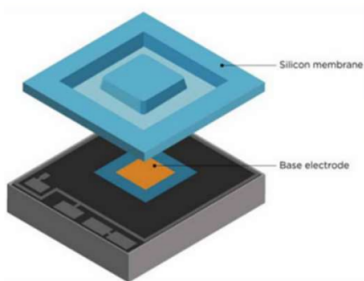


Figure 33: Pressure Sensor

Trace Species and Dust Sensor: The sensor is crucial for measuring the vertical distribution of dust aerosols and trace gases such as CH₄, H₂O, H₂O₂, and N₂O, providing insights into the boundary layer's composition

and dynamics. It employs multiple low-powered diode lasers and a multi-reflection optical cavity to detect extremely low concentrations. The sensor weighs 2 kg and requires around 20 W of power.

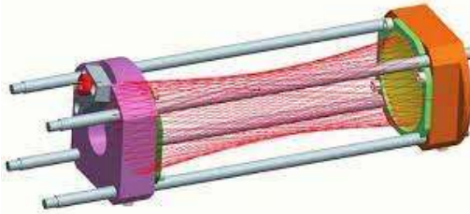


Figure 34: Herriott Cell-based Tunable Laser Spectrometer

Humidity Sensor: The sensor is essential for understanding H_2O distribution, near-surface ice stability, and Mars' habitability potential by measuring relative humidity in the near-surface layer. It uses an active polymer that changes capacitance with relative humidity. The sensor weighs 0.045 kg and requires about 0.02 W of power.

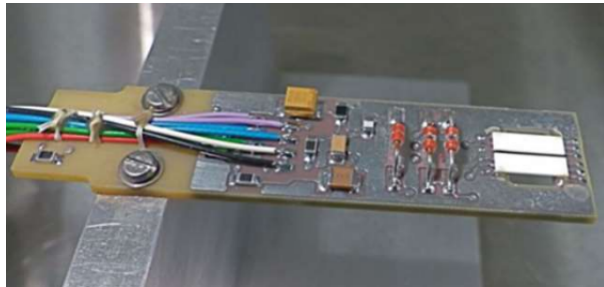


Figure 35: Humidity Sensor

Wind Sensor: The sensor is crucial for studying large-scale wind patterns, atmospheric waves, and dust storms, as well as for insights into future Mars aerial vehicles. It measures wind speed and direction in the near-surface layer and can be configured as a hot-wire anemometer, sonic anemometer, or laser Doppler anemometer. The sensor weighs about 1 kg and requires around 2 W of power.

Electric Field Sensor: The sensor is crucial for understanding dust particle frictional charging, which impacts atmospheric chemistry and dynamics. It measures the atmospheric electric field using a spherical electrode that detects the electric signal between the electrode and the UAV. The sensor weighs 1 kg and requires around 20 W of power.



Figure 36: Electric Field Sensor

It must be noted that the total mass of the payload is considered to be 5 kg , as stated in the problem statement, and the total payload power requirement is observed to be 42 W , which is rounded off to 50 W for the sake of power calculations. All the data mentioned in the section are referenced from the updated information on the payload sensors discussed in the 3rd Webinar of NACDeC-7 on the MARtian Boundary Layer (MARBLE) Payload Suite.

15 Energy Balance

A detailed overview of the energy consumed during the various phases of flight of the UAV is highlighted below.

| Phase of Flight | Energy (Wh) |
|-------------------------------|---------------|
| Climb | 132.35 |
| Hover | 5.11 |
| Descent | 123.71 |
| Total Power Consumed | 261.17 |
| Total Battery Capacity | 540 |

Figure 37: Energy Consumed

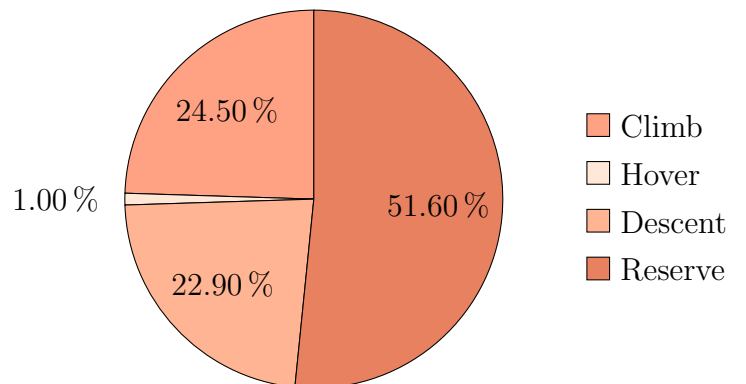


Figure 38: Energy Consumed

16 Mass Distribution

A detailed overview of the mass fraction of all the components used in the UAV is highlighted below.

| Component | Mass (kg) |
|------------------------------------|-----------|
| Avionics System | 3.5 |
| Battery Health Management System | 7 |
| Solar Panels (Including Mechanism) | 18 |
| Structure (Including Landing Gear) | 18 |
| Motors | 5 |
| Batteries | 3 |
| ESC | 1 |
| Payload | 5 |
| Propeller | 6 |
| Others | 3.5 |
| Total | 70 |

Figure 39: Mass Breakdown

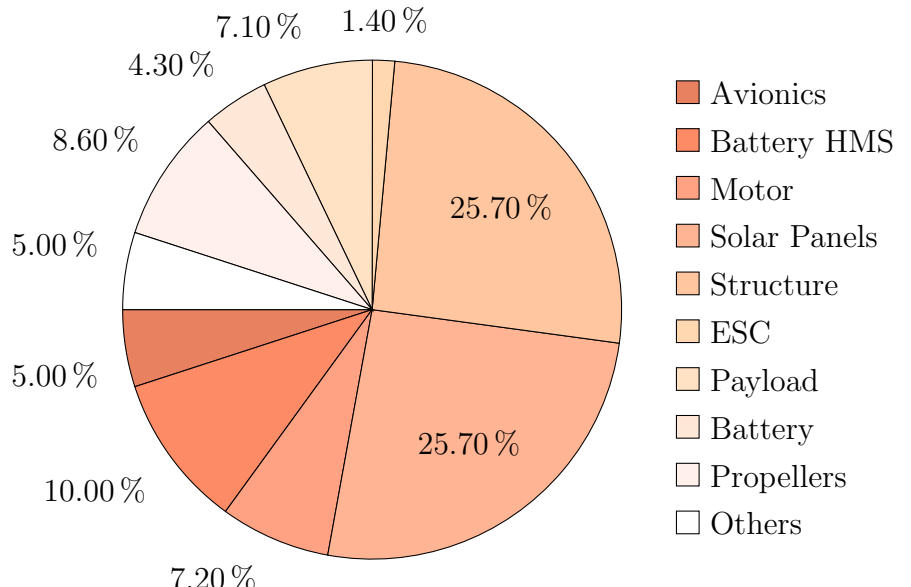


Figure 40: Mass Breakdown

17 Sample Calculations for Mission Timeline

This section details the calculations for battery charging time, current, and other key parameters for an accurate mission timeline using one battery-motor setup and the typical hover profile.

$$\text{Battery Ah} = \frac{1.5 \text{ kg} \times 180 \text{ Wh}}{100 \text{ V}} = 2.7 \text{ Ah} \quad (1)$$

In order to calculate the solar power being collected from the panels, the average irradiance during the charging period must be obtained first. This is done by assuming a certain time period, taking its average irradiance,

and then calculating the charge time it results in. If the charge time matches the earlier assumed time period, then we take it as the actual charging time or else repeat it till it matches. Therefore, the average irradiance between two time points, t_1 and t_2 , is given by:

$$\text{Avg. Irradiance} = \frac{Irr_1 + Irr_2}{2} \quad (2)$$

For this calculation, consider the 1st charging period from 06:02 to 08:02. Based on the solar irradiance variation over the Martian sol, the average irradiance during this period is approximately 48 W/m^2 . This average irradiance can then be used to calculate the solar power.

$$\text{Solar Power} = 17\% \times 25 \text{ m}^2 \times 48 \text{ W/m}^2 = 204 \text{ W} \quad (3)$$

The solar power from the panels will be evenly divided between the two batteries. The charging current for each battery is then calculated as follows:

$$\text{Charge Current} = \frac{0.5 \times 204}{100 \text{ V}} = 1.02 \text{ A} \quad (4)$$

The charge time of the battery can then be calculated in the following way,

$$\text{Charge Time} = \frac{\%DOD \times 2.7 \text{ Ah}}{1.02 \text{ A}} = 1.98 \text{ hrs} \quad (5)$$

It must be noted that %DOD was taken as 75% in this case because the UAV starts the mission day with only 25% reserve battery, and %DOD would be around 48% for other sortie cycles.

18 Final Mission Profile

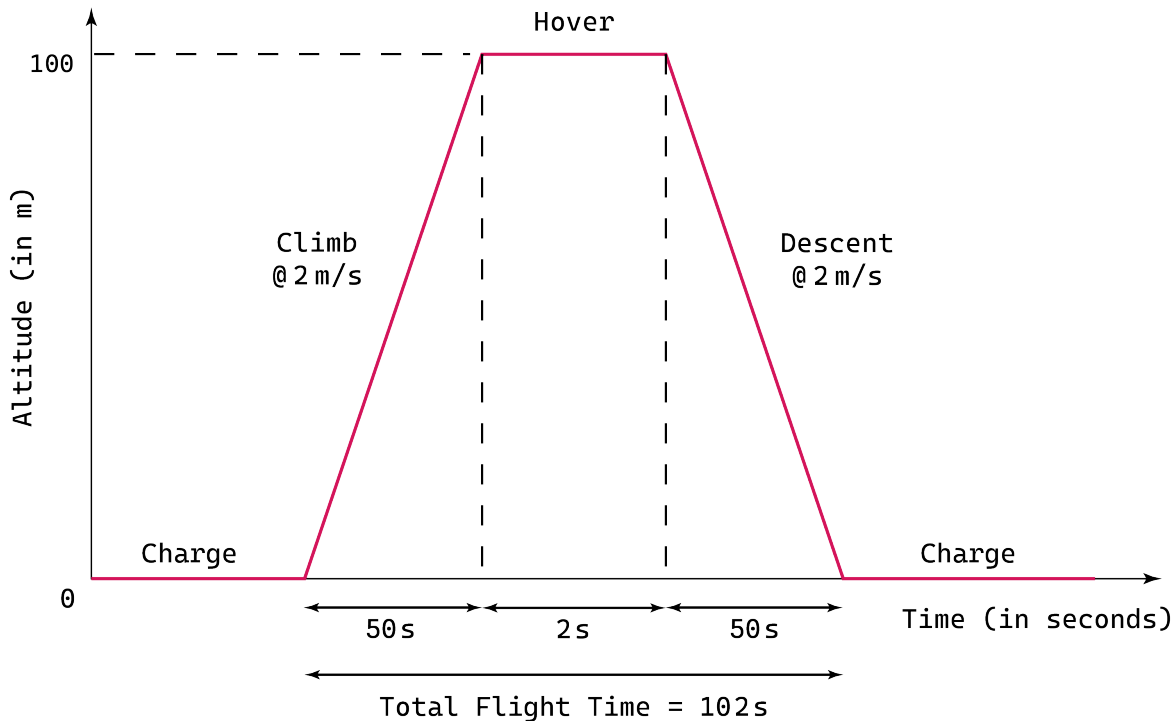


Figure 41: Mission Profile

19 Timeline of Sorties in a Martian Sol

| Time (hrs) | Activity | Time (hrs) | Activity |
|---------------|------------------------|---------------|------------------------|
| 06:00 - 06:02 | Solar Panel Deployment | 10:33 - 10:35 | 100s Wait |
| 06:02 - 08:02 | Charging | 10:35 - 10:37 | Solar Panel Retraction |
| 08:02 - 08:04 | 100s Wait | 10:37 - 10:39 | 6th Sortie |
| 08:04 - 08:06 | Solar Panel Retraction | 10:39 - 10:44 | Dust Settling Time |
| 08:06 - 08:08 | 1st Sortie | 10:44 - 10:46 | Solar Panel Deployment |
| 08:08 - 08:13 | Dust Settling Time | 10:46 - 10:56 | Charging |
| 08:13 - 08:15 | Solar Panel Deployment | 10:56 - 10:58 | 100s Wait |
| 08:15 - 08:45 | Charging | 10:58 - 11:00 | Solar Panel Retraction |
| 08:45 - 08:47 | 100s Wait | 11:00 - 11:02 | 7th Sortie |
| 08:47 - 08:49 | Solar Panel Retraction | 11:02 - 11:07 | Dust Settling Time |
| 08:49 - 08:51 | 2nd Sortie | 11:07 - 11:09 | Solar Panel Deployment |
| 08:51 - 08:56 | Dust Settling Time | 11:09 - 11:19 | Charging |
| 08:56 - 08:58 | Solar Panel Deployment | 11:19 - 11:21 | 100s Wait |
| 08:58 - 09:16 | Charging | 11:21 - 11:23 | Solar Panel Retraction |
| 09:16 - 09:18 | 100s Wait | 11:23 - 11:25 | 8th Sortie |
| 09:18 - 09:20 | Solar Panel Retraction | 11:25 - 11:30 | Dust Settling Time |
| 09:20 - 09:22 | 3rd Sortie | 11:30 - 11:32 | Solar Deployment Time |
| 09:22 - 09:27 | Dust Settling Time | 11:32 - 11:41 | Charging |
| 09:27 - 09:29 | Solar Panel Deployment | 11:41 - 11:43 | 100s Wait |
| 09:29 - 09:44 | Charging | 11:43 - 11:45 | Solar Panel Retraction |
| 09:44 - 09:46 | 100s Wait | 11:45 - 11:47 | 9th Sortie |
| 09:46 - 09:48 | Solar Panel Retraction | 11:47 - 11:52 | Dust Settling Time |
| 09:48 - 09:50 | 4th Sortie | 11:52 - 11:54 | Solar Panel Deployment |
| 09:50 - 09:55 | Dust Settling Time | 11:54 - 12:03 | Charging |
| 09:55 - 09:57 | Solar Panel Deployment | 12:03 - 12:05 | 100s Wait |
| 09:57 - 10:09 | Charging | 12:05 - 12:07 | Solar Panel Retraction |
| 10:09 - 10:11 | 100s Wait | 12:07 - 12:09 | 10th Sortie |
| 10:11 - 10:13 | Solar Panel Retraction | 12:09 - 12:14 | Dust Settling Time |
| 10:13 - 10:15 | 5th Sortie | 12:14 - 12:16 | Solar Panel Deployment |
| 10:15 - 10:20 | Dust Settling Time | 12:16 - 12:25 | Charging |
| 10:20 - 10:22 | Solar Panel Deployment | 12:25 - 12:27 | 100s Wait |
| 10:22 - 10:33 | Charging | 12:27 - 12:29 | Solar Panel Retraction |

Table 13: Timeline of the Mission Profile (since Sunrise)

| | | | |
|---------------|------------------------|---------------|------------------------|
| 12:29 - 12:31 | 11th Sortie | 14:53 - 14:55 | 17th Sortie |
| 12:31 - 12:36 | Dust Settling Time | 14:55 - 15:00 | Dust Settling Time |
| 12:36 - 12:38 | Solar Panel Deployment | 15:00 - 15:02 | Solar Panel Deployment |
| 12:38 - 12:47 | Charging | 15:02 - 15:20 | Charging |
| 12:47 - 12:49 | 100 s Wait | 15:20 - 15:22 | 100 s Wait |
| 12:49 - 12:51 | Solar Panel Retraction | 15:22 - 15:24 | Solar Panel Retraction |
| 12:51 - 12:53 | 12th Sortie | 15:24 - 15:26 | 18th Sortie |
| 12:53 - 12:58 | Dust Settling Time | 15:26 - 15:31 | Dust Settling Time |
| 12:58 - 13:00 | Solar Panel Deployment | 15:31 - 15:33 | Solar Panel Deployment |
| 13:00 - 13:10 | Charging | 15:33 - 15:56 | Charging |
| 13:10 - 13:12 | 100 s Wait | 15:56 - 15:58 | 100 s Wait |
| 13:12 - 13:14 | Solar Panel Retraction | 15:58 - 16:00 | Solar Panel Retraction |
| 13:14 - 13:16 | 13th Sortie | 16:00 - 16:02 | 19th Sortie |
| 13:16 - 13:21 | Dust Settling Time | 16:02 - 16:07 | Dust Settling Time |
| 13:21 - 13:23 | Solar Panel Deployment | 16:07 - 16:09 | Solar Panel Deployment |
| 13:23 - 13:33 | Charging | 16:09 - 16:49 | Charging |
| 13:33 - 13:35 | 100 s Wait | 16:49 - 16:51 | 100 s Wait |
| 13:35 - 13:37 | Solar Panel Retraction | 16:51 - 16:53 | Solar Panel Retraction |
| 13:37 - 13:39 | 14th Sortie | 16:53 - 16:55 | 20th Sortie |
| 13:39 - 13:44 | Dust Settling Time | 16:55 - 17:00 | Dust Settling Time |
| 13:44 - 13:46 | Solar Panel Deployment | 17:00 - 17:02 | Solar Panel Deployment |
| 13:46 - 13:57 | Charging | 17:02 - 18:18 | Charge |
| 13:57 - 13:59 | 100 s Wait | 18:18 - 18:20 | Solar Panel Retraction |
| 13:59 - 14:01 | Solar Panel Retraction | | |
| 14:01 - 14:03 | 15th Sortie | | |
| 14:03 - 14:08 | Dust Settling Time | | |
| 14:08 - 14:10 | Solar Panel Deployment | | |
| 14:10 - 14:22 | Charging | | |
| 14:22 - 14:24 | 100 s Wait | | |
| 14:24 - 14:26 | Solar Panel Retraction | | |
| 14:26 - 14:28 | 16th Sortie | | |
| 14:28 - 14:33 | Dust Settling Time | | |
| 14:33 - 14:35 | Solar Panel Deployment | | |
| 14:35 - 14:49 | Charging | | |
| 14:49 - 14:51 | 100 s Wait | | |
| 14:51 - 14:53 | Solar Panel Retraction | | |

Table 14: Timeline of the Mission Profile (till Sunset)



Team Name: FLIGHTFORGE
Manipal Institute of Technology

| Parameter | Value |
|-----------------------------|------------------|
| Total UAV Mass | 70 kg |
| Rotor Diameter | 5 m |
| Total Panel Area | 25 sq. m |
| No. of Solar Panel Sections | $11+11+2+1 = 25$ |

